Modal Dynamic Analysis of a Synchronizer Mechanism: A Numerical Study

A. Farokhi Nejad, G. Chiandussi, A. Moshrefzadeh
Politecnico di Torino, Department of Mechanical and Aerospace Engineering, Torino, Italy
Email: {ali.farokhi, giorgio.chiandussi, ali.moshrefzadeh} @polito.it

V. Solimine and A. Serra, E. Rulfi
Department of Design and virtual validation, Oerlikon Graziano, Torino, Italy
Email: {Vincenzo.Solimine, Andrea.Serra}@oerlikon.com

***Abstract*—The present paper shows the modal dynamic behaviour of a single cone synchronizer mechanism. A 3D finite element model is proposed to calculate the natural frequency of the system. By using an efficient method, the natural frequencies of every single component as well as the full system are extracted under different boundary conditions. The natural frequencies of the system in neutral and engaged conditions are extracted and the effective modes are identified. The finite element model is extended to evaluate transient response of the synchronizer mechanism. The effect of different boundary conditions on the modal response is presented. The results show that changing the actuator position can have a significant effect on the dynamic responses of the system. This methodology can be implemented to examine the transient behaviour of other shifting mechanisms.**

***Index Terms*—finite element model; natural frequency; synchronizer mechanism; Transient modal dynamics**

I. Introduction

Due to the global demands to reduce fuel consumption and emissions, many improvements have been implemented in automotive industry [1]. It has been investigated that based on the driving condition, up to 15% of energy loss originates from the transmission system [2]. In order to achieve environmental requirements and governmental regulations, the transmission systems in different categories have been introduced [3]. To obtain fast and smooth gear shifting, synchronizers often are utilized in automotive applications such as the manual transmission (MT), the automated manual transmission (AMT) and dual clutch transmission (DCT) systems [4]. Some studies have been conducted to investigate the effective parameters during the synchronization process, like the dynamic friction coefficient, thermal conditions, and the lubrication flow [5-7]. Moreover, different experimental test rigs were used to extract the overall behaviour of the shifting mechanism. However, those experimental rigs were not able to demonstrate the particular behaviour of every single component during the test. Therefore, some empirical models have been proposed to analyse the dynamic behaviour of the synchronizer [8-11]. The main difference between these models was the subdivision of the synchronization process into different phases. Moreover, numerical models have been implemented with a multi body dynamic (MBD) approach in order to evaluate the dynamic behaviour of synchronizer mechanism. Some MBD models have been developed to study the dynamic responses of synchronizer under different loading conditions [12, 13]. The synchronization time is one of the most important parameters of shifting process that can be estimated precisely with the proposed MBD model [14, 15].

Dynamic analysis of rotational systems such as geared systems is essential for reduction of noise and vibration. Some research have been conducted on natural frequencies and vibration modes of rotating machines such as automotive transmission systems, turbo engines, helicopter and etc. [16, 17]. Parker and his colleagues [18] have developed two different models to present some sources of nonlinearity in a planetary gear system. Walker et al. [19] have presented a lumped model to study the response of DCT powertrain during engagement process with and without engine harmonic-induced vibration. Although many studies have been performed on various components of the transmission systems [20, 21], less attention has been paid to the vibrational effects of the shifting mechanism. Since the synchronizer is involved transitionally in the dynamic behaviour of the transmission system, a transient analysis is needed to investigate the dynamic responses of the shifting mechanism. The objectives of the present study are: a) the development of a 3D finite element (FE) model suitable for extracting the natural frequency of a particular synchronizer and b) the evaluation of the effects of different boundary conditions on the dynamic response of the synchronizer mechanism.

II. Synchronization Process

The most common shifting mechanism for the transmission system is the Baulk ring-type mechanism equipped with a strut detent set [22]. This kind of synchronizer assembly includes a synchronizer hub, a

Manuscript received February 14, 2018; revised March 20, 2019.

doi: 10.18178/ijmerr.8.3.340-346

sliding sleeve, left and right synchronizer rings and friction cones, three strut detents, and left and right clutch body rings. The fork actuator is connected to the sliding sleeve groove to provide the axial load. Different parts of a single cone synchronizer and a sample of single cone synchronizer are shown in Fig. 1. The synchronizer mechanism is located between the two input and output shafts of the transmission system with different angular velocities and applied torques. In the neutral state, the input shaft is connected to the hub. In this step, the sliding sleeve, synchronizer ring, and strut detents have the same angular velocity as the input shaft and no axial displacement can be observed. However, the clutch body ring has a different rotational speed and applied torque. This phase can be called free-flying. Fig. 2 (a) shows the free-flying phase of the synchronization process. When the fork is actuated, the sliding sleeve starts moving to the synchronizer ring. In the second phase, the balls and springs that are inserted into the struts detents are compressed while they are sliding along the hub grooves.

Fig. 2 (b) shows the second phase of the synchronization process. By increasing the axial force, the first indexing between sliding sleeve and synchronizer ring teeth occurs. In this phase, the axial force transfers from fork and sleeve to the friction cone through strut detents. Fig. 2 (c) indicates the first indexing phase of the synchronization process. Due to stick contact between the clutch cone and synchronizer cone, the axial force raises to the maximum level at the synchronization phase that is shown in Fig. 2 (d). At the synchronization phase, the difference between input and output shaft becomes null. When the input and output velocities are the same, the final engagement process occurs that is shown in Fig. 2 (e).

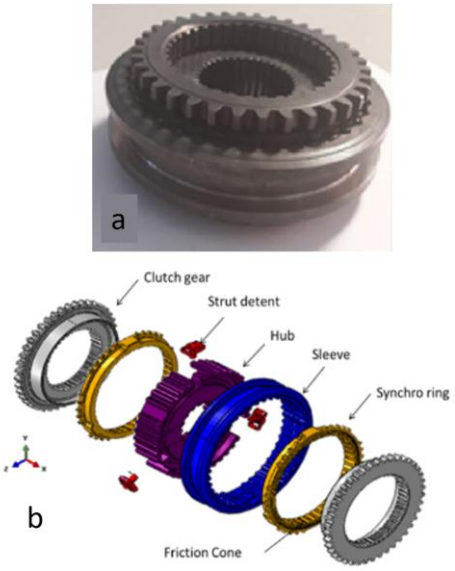

Figure1. (a) Single cone synchronizer sample and (b)the synchronizer components presented in an exploded view.

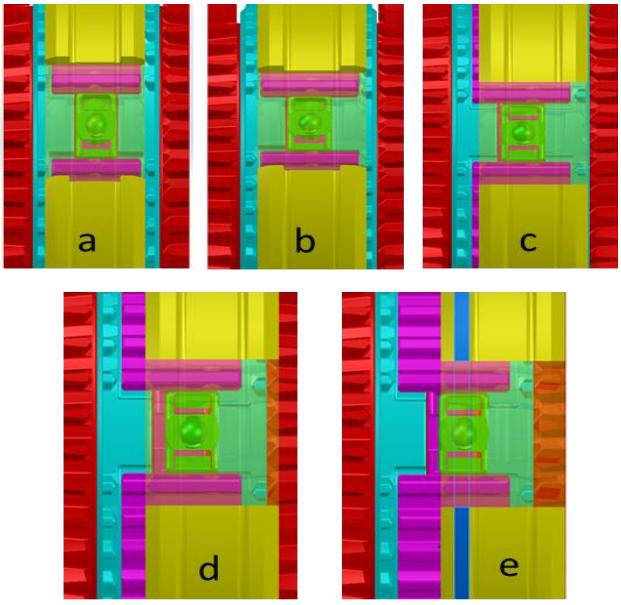

Figure 2. Different phases of the synchronization process (a) free-flying,(b) sliding sleeve motion,(c) first indexing (d) synchronization (e) final indexing and engagement.

III. Numerical Model

A. Mesh Convergence Study

To study the dynamic response of the synchronizer mechanism, a 3D geometry of the single cone synchronizer is imported to the ABAQUS commercial software. In order to verify the quality of the mesh, the natural frequencies of every separate part were calculated. The element type of all parts were the continuum solid element with 4 nodes and reduced integration ability. The eigenvalue problem for a finite element model can be calculated as:

$$(-\omega M^{MN} + K^{MN})\varphi^{N} = 0, \qquad (1)$$

where M^{MN} is the mass matrix, K^{MN} is the stiffness matrix regarding the initial stiffness effects, φ^{N} is the eigenvector (the mode of vibration); and M and N are degrees of freedom. To extract the natural frequency, the Automatic multi-level sub-structuring (AMS) Eigen solver was used. The AMS method consists of three steps. The first step includes a reduction process. In this step, a full system is reduced with a very efficient eigen solution method. This method combines sparse factorization based on the multilayer super node elimination tree and a local eigen solution at each super node. Starting from the lowest level super nodes, a Craig-Bampton substructure reduction technique is used to successively reduce the size of the system [23]. The second step consists of the reduced eigen problem solution. In this phase, the eigen solution of the reduced system that comes from the previous phase is calculated. Although the reduced system typically is two orders of magnitude smaller in size than the original system, generally it still is too large to be solved directly. Thus, the system is further reduced mainly by truncating

the retained eigen modes and then solved using a single subspace iteration step. The last step is recovery. In this phase, the eigenvectors of the original system are recovered using eigenvectors of the reduced problem and local substructure modes [24]. All simulations were performed in the free-free condition. The material properties of all parts for natural frequency analysis were considered as linear elastic. Figures 3(a) to 3(e) show the natural frequencies of every component by reducing the element size till reaching a stable solution. In all cases, 10 modes are illustrated. At the end of the mesh convergence analysis, the element suitable size of each part is shown in Table I.

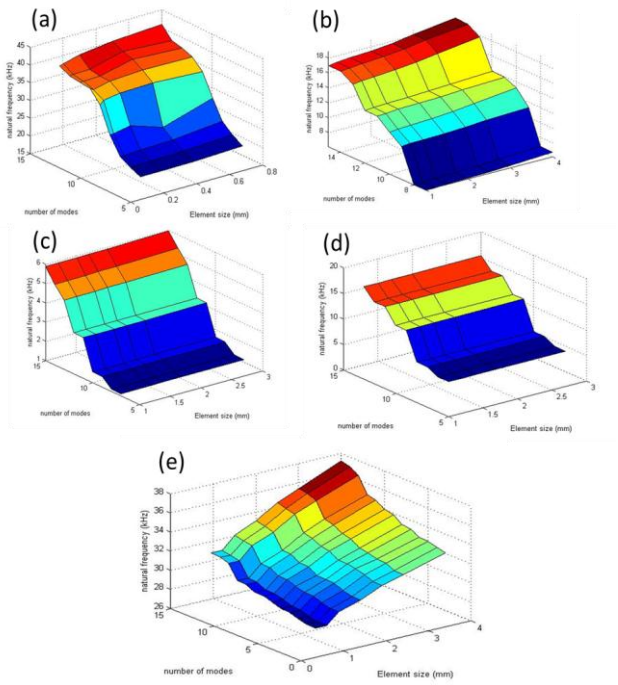

Figure 3. Mesh convergence study and natural frequency of separate parts (a) Strut detent (b) Synchronizer hub (c) Synchronizer ring (d) Clutch body ring (e) Sliding sleeve.

TABLE I. THE MESH CONFIGURATION OF SEPARATE PARTS OF THE SYNCHRONIZER.

component	Converged element size (mm)	Number of element
Strut detent	0.18	6056
Synchronizer hub	1	61041
Synchronizer ring	1	51803
Clutch body ring	1.5	75758
Sliding sleeve	0.95	102883

B. Natural Frequency of the Full System with Free Boundary Conditions

Once the appropriate mesh size for each component has been identified, the full model is assembled in two different working conditions: neutral state and engaged state. The AMS eigen solver also is used to calculate the natural frequencies of the synchronizer. A surface to surface contact pair algorithm was implemented in all contact areas. Due to the fact that the synchronizer works in a low frequency range, ten initial mode shapes are requested and the natural frequencies of the system are extracted with free boundary conditions. Figure 4 shows the different mode shapes of the synchronizer in the neutral working condition.

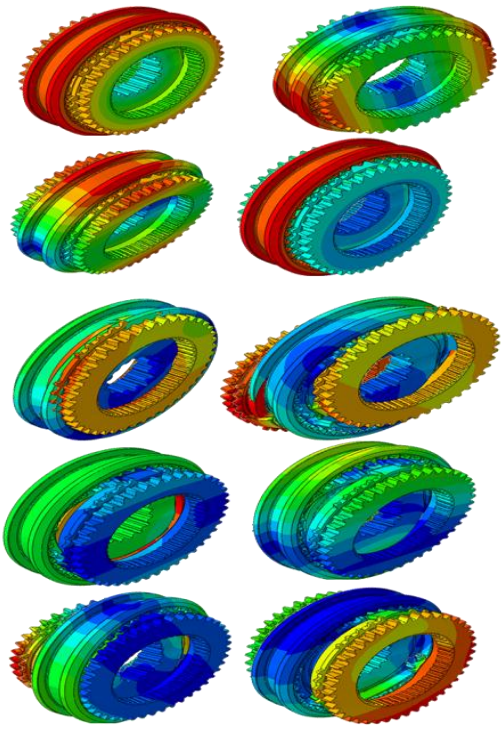

Figure 4. Different mode shapes of single cone synchronizer in free-free condition.

It can be seen that the three initial mode shapes are related to rigid modes. From the fourth mode on, the deformable modes of the system can be observed. Figure 5 compares the natural frequencies obtained by the analysis of the neutral and the engaged working conditions for the single cone synchronizer with free-free boundary conditions. In this figure, the rigid and flexible modes are presented clearly. Changing the position of the sliding sleeve and changing from neutral condition, to the engaged condition a stiffer system is obtained and its natural frequencies increase.

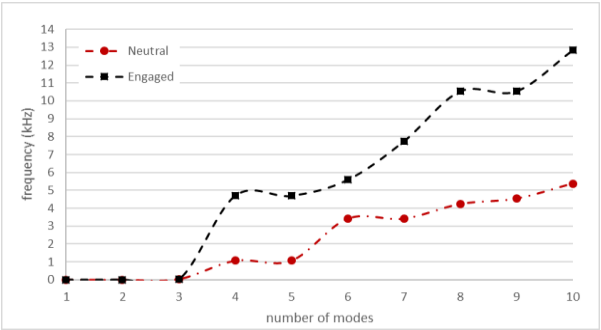

Figure 5. Natural frequency of the single cone synchronizer in neutral and engaged conditions with free-free boundary conditions.

C. Natural Frequency of the Full System with Constraint Boundary Coditions

Since the synchronizer mechanism is mounted between the input and output shafts, the input and output shafts should be considered to study the natural frequencies of the system. Based on the application of this specific synchronizer, four different conditions can be considered as a case study. Figure 6 shows the schematic of a synchronizer set with assembled input and output shafts. The end side of the left shaft is free to rotate and also free to move axially (Ux, URx ≠0). The end of the right shaft is only free to rotate (URx≠0). Table 2 presents the different boundary conditions of the single cone synchronizer.

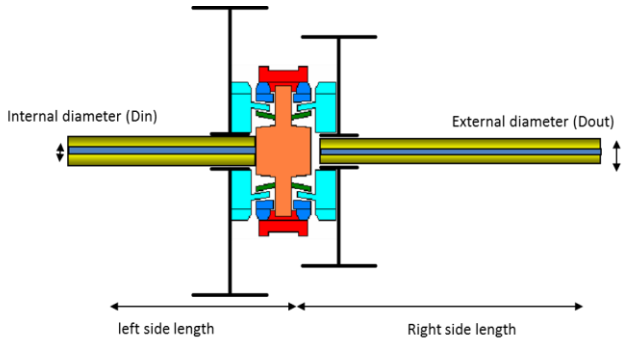

Figure 6. The schematic of a synchronizer set with assembled input and output shafts.

TABLE II. THE DIMENSION OF CONNECTING SHAFTS OF SYNCHRONIZER MECHANISM

Boundary conditions	Shaft diameter(mm)		Shaft length (mm)	
	Internal diameter	*External diameter*	*Left side*	*Right side*
Lmax-Dmin	12	34	172	69
Lmax-Dmax	18	47	172	69
Lmin-Dmin	12	34	56	75
Lmin-Dmax	18	47	56	75

In order to reduce the time of calculation, the shafts were modelled with 3D beam element (B31) and the size of elements for all models is considered 0.5 mm. Given that natural frequencies of the fully engaged system are larger than the range of interest, natural frequencies of the system in a neutral state were considered. Figure 7 compares natural frequencies of the single cone synchronizer subject to different boundary conditions.

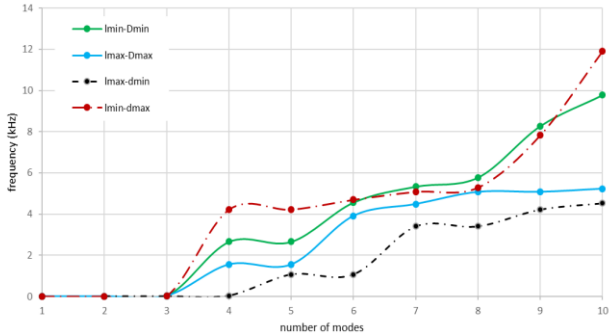

Figure 7. The effect of different boundary conditions on the natural frequency of the neutral position.

IV. MODAL DYNAMIC RESPONSES

A. Dynamic Equation

As mentioned in the previous section, given the transient behaviour of the synchronizer, it is necessary to perform the modal transient analysis to examine the dynamic response of the system. In order to analyse a linear system, the dynamic equation for a time response problem can be written as:

$$[M]_\beta[\ddot{u}]_\beta + [C]_{\beta\alpha}[\dot{u}]_\alpha + [K]_\beta[u]_\beta = (f_t)_\beta \quad (2)$$

where M is the mass matrix, C is the viscous damping matrix, K is the stiffness matrix, α and β indices span the eigen space and U is the generalized displacement of the mode β. The substitution of ω= √ (K⁄M) in (2) yields:

$$[\ddot{u}]_\beta + [C]_{\beta\alpha}[\dot{u}]_\alpha + \omega^2[u]_\beta = (f_t)_\beta \quad (3)$$

Moreover, to simplify the (3) the ζ_β (damping ratio) can be calculated as:

$$2\zeta_\beta\omega_\beta = \frac{C_\beta}{M_\beta} \quad (4)$$

and the full system dynamic equation with diagonal damping matrix can be written as:

$$[\ddot{u}]_\beta + 2\zeta_\beta\omega_\beta[\dot{u}]_\alpha + \omega^2[u]_\beta = (f_t)_\beta \quad (5)$$

However, for a coupled system, the viscous damping matrix should be split into the diagonal and off-diagonal matrix as follow:

$$C = C_{diag} + C_{off} \quad (6)$$

The solution to the coupled equations is obtained readily as a particular integral for the loading and a solution to the homogeneous equation. These solutions can be combined and written in the general form:

$$\begin{Bmatrix} u_t+\Delta t \\ \bar{C}\dot{u}_t+\Delta t \end{Bmatrix} = \begin{bmatrix} a_{11} & a_{12}-b_{11}C_{off} \\ a_{21} & a_{22}-b_{21}C_{off} \end{bmatrix} \begin{Bmatrix} u_t \\ \dot{u}_t \end{Bmatrix} + \begin{bmatrix} b_{11} & b_{12} \\ b_{21} & b_{22} \end{bmatrix} \begin{Bmatrix} u_t \\ \dot{u}_t \end{Bmatrix} + \begin{bmatrix} 0 & -b_{11}C_{off} \\ 0 & 0 \end{bmatrix} \begin{Bmatrix} u_t+\Delta t \\ \dot{u}_t+\Delta t \end{Bmatrix} \quad (7)$$

Since the loading only varies linearly over the time increment *(Δf⁄Δt)*, The a_{ij} and b_{ij} are constants and *i,j*=1,2. To calculate *a* and *b* constants in more detail see [23].

B. 3d Finite Element Model for Modal Analysis

The previous model is extended to examine the modal dynamic behaviour of the single cone synchronizer. In this case, the model is obtained in two different steps. The first step is the same as the previous model and is used for the natural frequency extraction. In the second step, a time response analysis was performed and the FE results are converted into the frequency domain by using Fast Fourier Transform (FFT). In the first step, only shafts were constrained as in the previous model. The clutch body ring and the hub are free to rotate (URx ≠0) and synchronizer rings and sliding sleeve are free to rotate and

move axially (Ux, URx ≠ 0). The surface to surface contact algorithm was implemented for every contact surface pair. The friction coefficient between clutch body ring and synchronizer ring was considered 0.06. Figure 8 shows the finite element model used for modal analysis.

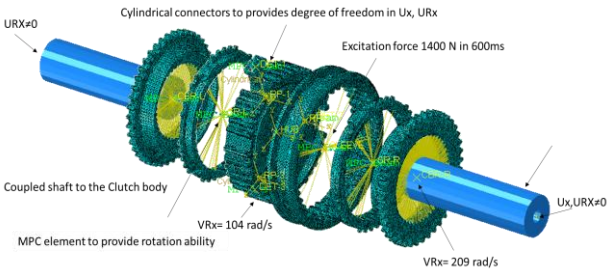

Figure 8.The FE model for modal dynamic analysis of synchronizer mechanism.

The AMS eigen solver is used for natural frequency calculation in the first step. Similar to previous section, ten modes were requested. The second step uses the extracted natural frequencies to compute the transient response of the system that is excited with a ramped force. Figure 9 shows the applied load as the excitation force in a short period of time. The loading time was taken from a previous study [14]. The damping ratio in this study was set to 0.05.

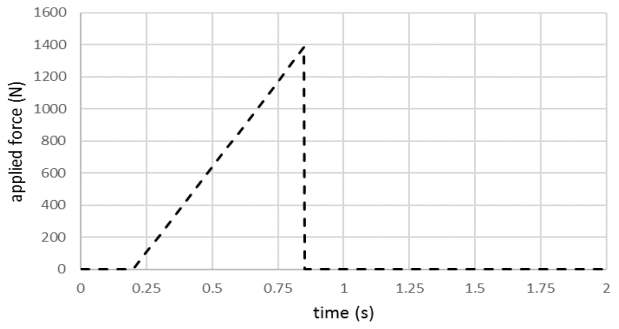

Figure 9. The applied force to the sliding sleeve for system excitation.

Since the range of frequencies for single cone synchronizer is between 0 and 100 Hz, only five modes are used for the second step. The rotational speeds to the synchronizer hub and clutch body ring were allocated. The synchronizer hub is rotating with 104 rad/s and clutch body rings are rotating with 209 rad/s. After actuating the sliding sleeve with the excitation force, the result of time response solver converted to the frequency response by using FFT plot. Figure 10 illustrates the frequency response of the synchronizer with different boundary conditions.

C. *Effect of Actuator Position on the Dynamic Response*

Due to manufacturing aspects, the fork and sliding sleeve can be installed in their position with allowable tolerance. However, this small displacement can affect the stiffness matrix of the system. For this reason, the minimum, maximum and nominal size were applied to the sliding sleeve position. Table 3 shows all resonance frequencies and corresponding amplitudes for different conditions. It can be seen that the worst case is related to Lmax-Dmax boundary conditions.

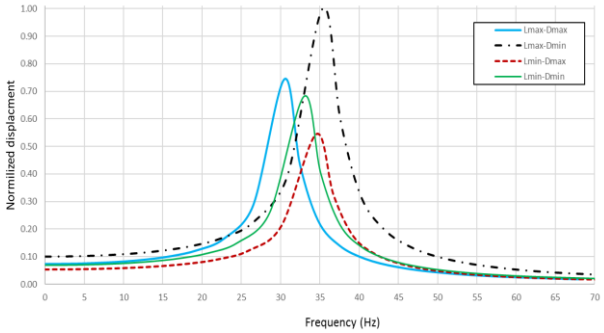

Figure 10. The frequency response of the single cone synchronizer with different bounday conditions.

TABLE III. THE DYNAMIC SYSTEM CHARACTERS WITH DIFFERENT BOUNDARY CONDITIONS AND SLIDING SLEEVE CLEARANCE.

Applied boundary conditions	Sleeve position					
	min		*nom*		*max*	
	freq (Hz)	*amp (μ)*	*freq (Hz)*	*amp (μ)*	*freq (Hz)*	*amp (μ)*
Lmin-Dmax	27	51.9	34.6	27.2	35.8	28.8
Lmin-Dmin	29.1	54.5	33	34.1	37.2	37.1
Lmax-Dmax	29.6	67.5	30.5	37.5	32.5	53
Lmax-Dmin	34.1	57.7	35.2	50	39.2	38.6

Fig. 11 compares the dynamic response for different sleeve's positions with Lmax-Dmin boundary condition. When the sliding sleeve is in the minimum condition, it means that the minimum clearance between sliding sleeve teeth and the synchronizer ring teeth has existed.

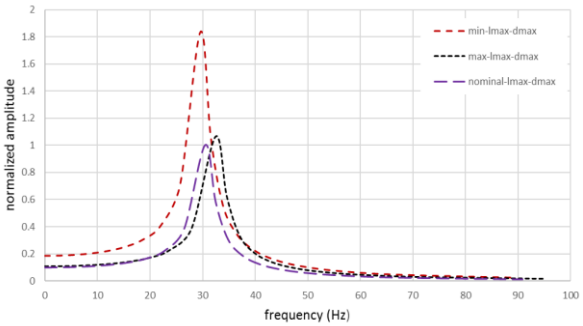

Figure 11. The effect of different clearances between sleeve and the synchronizer ring on the frequency response of single cone synchronizer.

V. DISCUSSION AND CONCLUSION

The present study introduces the synchronizer mechanism and different phases of synchronization. To better understand the dynamic behaviour of the synchronizer, the study of the modal and natural frequencies of the mechanism is essential. For this reason, in the first step, natural frequencies of each component were calculated. In order to achieve more accurate numerical results, the mesh convergence study was

applied to every single part. Furthermore, the synchronizer mechanism was assembled with the converged element size. The natural frequencies of the full system in the neutral and engaged conditions were calculated by AMS method. The results show that when the mechanism is engaged, the system stiffness increases and the natural frequencies of the system become higher than the frequency range of interest. However, the synchronizer is connected to the input and output shafts and the stiffness of connected shafts affects the natural frequencies of the system. Therefore, the connecting shafts were added to the FE model and natural frequencies of all four possible boundary conditions were extracted. Increasing the length and decreasing the diameter of the shafts, the natural frequencies of the system decrease. The lowest natural frequency is obtained in the Lmax-Dmin combination.

After calculation of the natural frequencies of the synchronizer, the FE model is extended to study the effect of excitation force and transient modal response of the synchronizer. A ramped force as the excitation force was applied to the sliding sleeve and time responses of the system with different boundary condition were estimated. The results show that the worst case is Lmax-Dmin with 50 μm at 35.2 Hz: the maximum deflection occurs when the resonance mode is equal to 35.2 Hz.

By changing the sliding sleeve position, the clearance between the sleeve teeth and the synchronizer ring teeth can be varied. This variation can occur due to the manufacturing process. The effect of backlash between teeth pair was examined for all possible boundary conditions. Surprisingly, when the sleeve backlash is in minimum allowable tolerance, the critical amplitude is changed from Lmax-Dmin to the Lmax-Dmax. The minimum clearance between sleeve and synchronizer ring increases the maximum amplitude more than 1.8 times than nominal clearance. Comparison between different conditions shows that the backlash effect dominates the effect of the shafts boundary conditions.

The proposed model can be used for the evaluation of dynamic responses of different types of synchronizer subject to different loading and boundary conations. Moreover, the dynamic parameters of the single cone synchronizer such as natural frequency, maximum amplitude, resonance frequency and effective boundary conditions were characterized.

ACKNOWLEDGMENT

The authors gratefully acknowledge industrial partner Oerlikon Graziano for the financial and technical support of this ongoing project.

REFERENCES

[1] A. F. Nejad, S. Peirovi, and M. N. Tamin, "Computational aided design for generating a modular, lightweight car concept," arXiv preprint arXiv:1711.10782, 2017.

[2] A. Irimescu, L. Mihon, and G. Pădure, "Automotive transmission efficiency measurement using a chassis dynamometer," *International Journal of Automotive Technology*, vol. 12, no. 4, pp. 555-559, 1229-9138, 2011.

[3] G. Poll and M. Spreckels, "Influence of temperature distribution on the tribological performance of automotive synchronisers," in *Tribology Series*, vol. 41: Elsevier, 2003, pp. 613-621 0167-8922.

[4] C. Y. Tseng and C. H. Yu, "Advanced shifting control of synchronizer mechanisms for clutchless automatic manual transmission in an electric vehicle," *Mechanism and Machine Theory*, vol. 84, pp. 37-56, 0094-114X, 2015.

[5] A. Sandooja and S. Jadhav, "Analysis of gear geometry and durability with asymmetric pressure angle," *SAE International Journal of Commercial Vehicles*, vol. 5, no. 2012-01-1995, pp. 546-558, 1946-3928, 2012.

[6] B. Paffoni, R. Progri, R. Gras, and J. Blouët, "The hydrodynamic phase of gearbox synchromesh operation: The influence of radial and circumferential grooves," in *Proc. the Institution of Mechanical Engineers, Part J: Journal of Engineering Tribology*, vol. 211, no. 2, pp. 107-116,1350-6501, 1997.

[7] G. Yuming, "Discuss designing-method of transmission synchronizer," 2011.

[8] Y. C. Liu and C. H. Tseng, "Simulation and analysis of synchronisation and engagement on manual transmission gearbox," *International Journal of Vehicle Design*, vol. 43, no. 1-4, pp. 200-220 , 0143-3369, 2007.

[9] L. Lovas, D. Play, J. Marialigeti, and J. F. Rigal, "Mechanical behaviour simulation for synchromesh mechanism improvements," in *Proc. the Institution of Mechanical Engineers, Part D: Journal of Automobile Engineering*, vol. 220, no. 7, pp. 919-945, 0954-4070, 2006.

[10] S. T. Razzacki, "Synchronizer design: A mathematical and dimensional treatise," ed: SAE Technical Paper, 2004.

[11] M. K. Sharma and J. Savla, "Shift system inertia mass optimization techniques to minimize double bump for manual transmission," ed: SAE Technical Paper, 2012.

[12] H. Hoshino, "Analysis on synchronization mechanism of transmission," ed: SAE Technical Paper, 1999.

[13] H. Golbach, "The application of modern FE simulation methods in the product development of transmission components," ed: SAE Technical Paper, 2004.

[14] A. Farokhi and G. Chiandussi, "Estimation of the synchronization time of a transmission system through multi body dynamic analysis," *International Journal Of Mechanical Engineering And Robotics Research*, vol. 6, no. 3, pp. 232-236, 2278-0149, 2017.

[15] A. Farokhi Nejad, G. Chiandussi, V. Solimine, and A. Serra, "Study of a synchronizer mechanism through multibody dynamic analysis," in *Proc. the Institution of Mechanical Engineers, Part D: Journal of Automobile Engineering*, p. 0954407018772238.

[16] G. W. Blankenship and A. Kahraman, "Steady state forced response of a mechanical oscillator with combined parametric excitation and clearance type non-linearity," *Journal of Sound and Vibration*, vol. 185, no. 5, pp. 743-765, 0022-460X, 1995.

[17] A. Kahraman and G. W. Blankenship, "Experiments on nonlinear dynamic behavior of an oscillator with clearance and periodically time-varying parameters," *Journal of Applied Mechanics*, vol. 64, no. 1, pp. 217-226, 0021-8936, 1997.

[18] V. K. Ambarisha and R. G. Parker, "Nonlinear dynamics of planetary gears using analytical and finite element models," *Journal of Sound and Vibration*, vol. 302, no. 3, pp. 577-595, 0022-460X, 2007.

[19] P. D. Walker and N. Zhang, "Investigation of synchroniser engagement in dual clutch transmission equipped powertrains," *Journal of Sound and Vibration*, vol. 331, no. 6, pp. 1398-1412 %@ 0022-460X, 2012.

[20] Y. Zhang, X. Chen, X. Zhang, H. Jiang, and W. Tobler, "Dynamic modeling and simulation of a dual-clutch automated lay-shaft transmission," *Journal of Mechanical Design*, vol. 127, no. 2, pp. 302-307, 1050-0472, 2005.

[21] R. G. Parker, V. Agashe, and S. M. Vijayakar, "Dynamic response of a planetary gear system using a finite element/contact mechanics model," *Journal of Mechanical Design*, vol. 122, no. 3, pp. 304-310, 1050-0472, 2000.

[22] L. Lovas, D. Play, J. Márialigeti, and J.-F. Rigal, "Modelling of gear changing behaviour," *Periodica Polytechnica.*

Transportation Engineering, vol. 34, no. 1-2, pp. 35, 0303-7800, 2006.

[23] P. Gerds and L. Grasedyck, "Solving an elliptic PDE eigenvalue problem via automated multi-level substructuring and hierarchical matrices," *Computing and Visualization in Science*, vol. 16, no. 6, pp. 283-302, 1432-9360, 2013.

[24] V. Abaqus, "6.14 Documentation," Dassault Systemes Simulia Corporation, 2014.

Ali Farokhi Nejad received the B.S. and M.S. in Mechanical Engineering from Iran and Universiti Teknologi Malaysia, respectively. He is currently a Ph.D. candidate in Department of Mechanical and Aerospace engineering, Politecnico di Torino.

Giorgio Chiandussi received the B.S. and M.S. and Ph.D. in Mechanical Engineering from Politecnico di Torino, Italy. He is currently a Professor in the Faculty of Mechanical and Aerospace Engineering, Politecnico di Torino.

Vincenzo Soilimine received the B.S. and M.S. in Mechanical Engineering from Universit à degli Studi di Napoli. Currently he is a Research engineer in Department of Design and virtual validation, Oerlikon Graziano, Torino, Italy

Andrea Serra was graduated from Department of Mechanical and Aerospace engineering, Politecnico di Torino.Currently he is the head of the Department of Design and virtual validation, Oerlikon Graziano, Torino, Italy

Ali Moshrefzadeh received the B.S. and M.S. in Mechanical Engineering from Iran. He received his Ph.D. from Department of Mechanical and Aerospace engineering, Politecnico di Torino. He is currently research assistant in Politecnico di Torino.

E. Rulfi was graduated from Department of Mechanical and Aerospace engineering, Politecnico di Torino.Currently he is project engineer at Department of Design and virtual validation, Oerlikon Graziano, Torino, Italy